Nuclear Instruments and Methods in Physics Research A 671 (2012) 1–5

Contents lists available at SciVerse ScienceDirect

Nuclear Instruments and Methods in Physics Research A

journal homepage: www.elsevier.com/locate/nima

New measurement technique for the product of the electron mobility and mean free drift time for pixelated semiconductor detectors

Yvan A. Boucher*, Feng Zhang, Willy Kaye, Zhong He

Department of Nuclear Engineering and Radiological Science, University of Michigan, Ann Arbor, MI 48109, USA

ARTICLE INFO

Article history:
Received 26 April 2011
Received in revised form
1 December 2011
Accepted 3 December 2011
Available online 24 December 2011

Keywords:
Semiconductor detector
CdZnTe
Gamma ray detector

ABSTRACT

A new method for measuring the electron mobility, the electron mean free drift time, and their product has been developed for pixelated semiconductor detectors. Using data from a standard calibration measurement, these three quantities are measured and compared against results using other methods. Since the results can be easily obtained, comparisons of many detectors have been completed and show that detector spectroscopic performance is independent of the electron trapping if the raw electron trapping is less than 6.5% from the cathode to the anode surface.

1. Introduction

Thorough understanding of the characteristics of charge carrier transport in a semiconductor detector is important for determining the material quality and the overall detector performance. Two typical quantities to characterize the charge transport are the electron mobility (μ_e) and the mean free drift time (τ_e). The derived quantity of $\mu_e\tau_e$ is a common metric for studying semiconductor properties.

Typical methods for measuring $\mu_e\tau_e$ are conducted using α-particle spectroscopy and are based on the Hecht relation [1]. However, methods based on the Hecht relation tend to be biased towards lower value of $\mu_e\tau_e$ due to ballistic deficit and surface trapping [2]. Therefore a direct measurement technique based on single polarity charge sensing can be used to improve the determination of $\mu_e\tau_e$ [2]. Single polarity charge sensing is a technique developed for detector materials, such as CdZnTe or HgI_2, where the mobility of holes is several orders of magnitude less than the mobility of the electrons [3]. Therefore, the induced signal measured from the crystal will be entirely due to the movement of the electrons as the holes are virtually stationary during the electron drift.

The technique described in Ref. [2] uses measurements of charge collection at different voltages to determine the value of $\mu_e\tau_e$. This technique has been altered to utilize the standard calibration data acquired for a pixelated semiconductor detector. A standard calibration measurement is routinely made for each detector to characterize its spectroscopic performance; therefore, a technique to utilize this measurement to determine $\mu_e\tau_e$ will allow for a more thorough comparison between charge transport properties and spectroscopic performance without requiring an additional experimental effort. This new technique has allowed for the comparison between $\mu_e\tau_e$ and energy resolution for 35 $2\times2\times1.5$ cm^3 CdZnTe detectors recently received from Redlen Technologies, Inc. Comparable results for 1 cm^3 CdZnTe detectors grown by Redlen Technologies, Inc. have been found using a technique based on the Hecht relation [3]. Other research groups using the Hecht relation to measure the electron mobility-lifetime product have also found comparable results [4].

2. Methodology

For each $2\times2\times1.5$ cm^3 CdZnTe detector a calibration measurement is taken to correct the signal amplitude for each anode pixel to determine its spectroscopic capabilities. These detectors are pixelated with 121 anode pixels and contain a steering grid. All tests were conducted at room temperature using identical procedures with readout electronics from Gamma Medica-Ideas, including the GMI VAS_UM2.3TAT4 application specific integrated circuit (ASIC) [5]. The standard 3-D energy calibration requires acquiring sufficient counts throughout the entire detector volume to accurately determine the signal amplitude of a full energy deposition from a 662 keV Cs-137 gamma ray [6]. The detector is typically separated into 40 depth bins along with the 121 anode pixels, resulting in an individual 3-D energy calibration for each of the 4840 detector voxels for which a single interaction could occur within. Therefore, raw single-pixel energy spectra are

* Corresponding author.
E-mail address: yanders@umich.edu (Y.A. Boucher).

0168-9002/$ - see front matter © 2011 Elsevier B.V. All rights reserved.
doi:10.1016/j.nima.2011.12.008

collected as a function of the three dimensional interaction location. An example of the spectra for a single pixel exhibiting the amplitude suppression due to electron trapping is shown in Fig. 1. Taking advantage of the relatively constant anode signal amplitude due to the small pixel effect and the depth-sensitive cathode signal amplitude, the cathode-to-anode signal ratio is used to determine the depth of interaction [7]. For each voxel, a raw photopeak energy centroid and raw timing peak centroid—which is an independent measure of the depth of interaction—are found.

The mean free drift time, the mobility, and their product can now be calculated from the information obtained from each voxel. From Eq. (1) for the signal amplitude deficit resulting from electron trapping losses, the electron mean free drift time, τ_e, can be derived as shown in Eq. (2):

$$N = N_0 \times e^{-t/\tau_e} \tag{1}$$

$$\tau_e = \frac{(t_2 - t_1)}{\ln(N_2/N_1)} \tag{2}$$

where τ_e is the electron mean free drift time, t is the drift time, and N is the raw photopeak energy centroid.

The drift time between two vertical positions within a pixel in the detector can be determined from the drift time versus depth relationship for that pixel. An example relationship for a single pixel is shown in Fig. 2, which shows that the depth of interaction can be uniquely mapped to drift time. The non-linearity of the depth of interaction to drift time mapping can be primarily attributed to a non-uniform electric field near the anode and cathode surfaces. To limit the effect of electric field non-uniformity, the center region of the detector which has the best linearity is used to determine τ_e—depths ranging from 7.5 mm to 13.125 mm. Therefore, the relationship between the photopeak energy centroid and depth can be used to determine τ_e through mapping each depth to its unique drift time. The relationship between photopeak centroid and depth is shown for a single pixel in Fig. 3.

The electron mobility, μ_e, is calculated from solving Eq. (3). Any non-uniformity in the electric field is accounted for by integrating the velocity, v, and electric field, E, over the depth, z, as shown in Eq. (4). The final result, Eq. (5), gives μ_e as a function of the velocity and the magnitude of the Voltage, V, in that region of the detector. The non-linearity in the drift time versus depth relationship shown in Fig. 2 is accounted for by integrating over the depth:

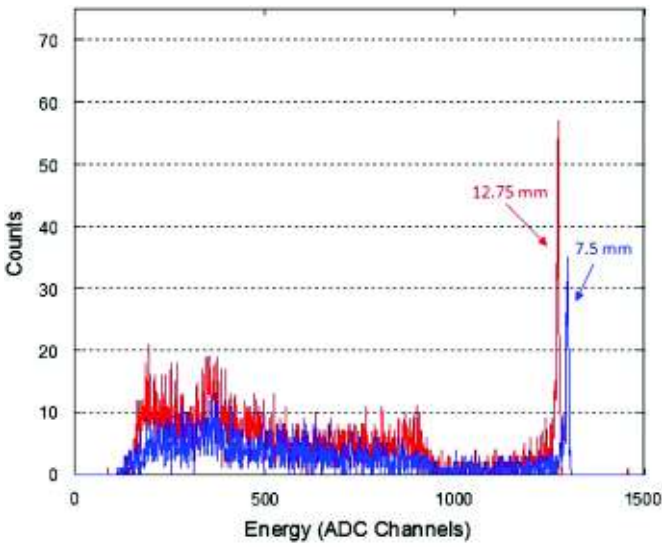

Fig. 1. Energy spectra showing the electron loss due to charge trapping between two different interaction depths (7.5 and 12.75 mm relative to the anode) within a single pixel of a 15 mm thick CdZnTe detector.

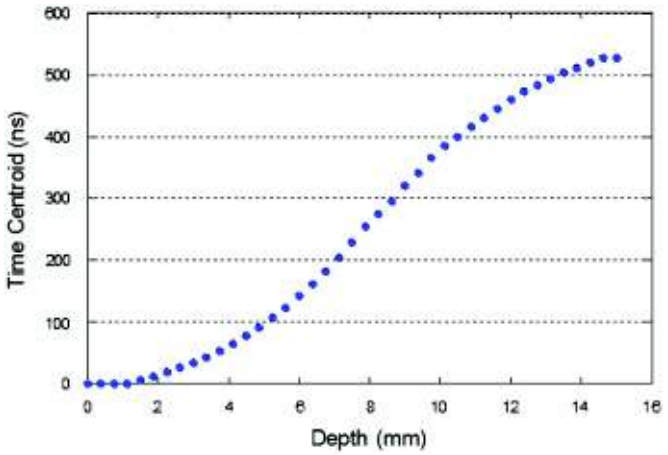

Fig. 2. Relationship for the drift time versus the depth of interaction that is used to uniquely map drift time to depth. The depth of interaction is determined using the cathode-to-anode signal ratio.

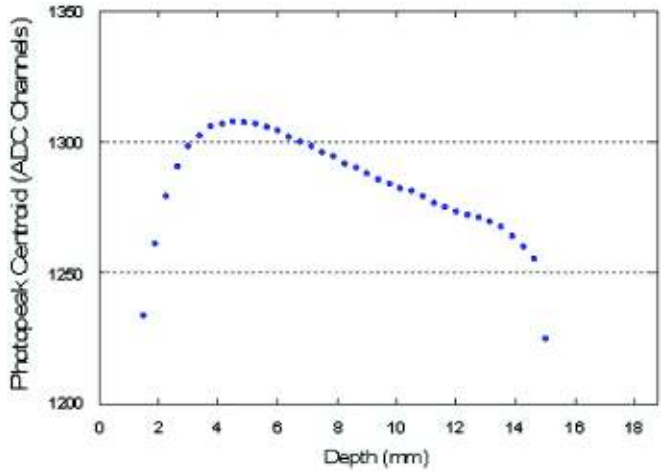

Fig. 3. Relationship between photopeak centroid and depth of interaction that is used to determine τ_e and $\mu_e\tau_e$. Again, the depth of interaction is determined using the cathode-to-anode signal ratio.

$$v = \mu_e E \tag{3}$$

$$\int_{z=7.5\text{ mm}}^{13.125\text{ mm}} v \cdot dz = \mu_e \int_{z=7.5\text{ mm}}^{13.25\text{ mm}} E \cdot dz = \mu_e \cdot V \cdot x \tag{4}$$

$$\mu_e = \frac{1}{V \cdot x} \int v \cdot dz = \frac{1}{V \cdot x} \sum_{i=7.5\text{ mm}}^{13.125\text{ mm}} \frac{z_{i+1} - z_i}{t_{i+1} - t_i}\, dz \tag{5}$$

where μ_e is the electron mobility, dz is the width of the depth bins (0.375 mm), and x is a scaling factor to account for the limits of integration. The scaling factor x is equal to the depth range divided by the total thickness, or 5.625 mm/15 mm=0.375.

The electron mobility and mean free drift time can then be multiplied to find $\mu_e\tau_e$, as shown in the following equation:

$$\mu_e\tau_e = \frac{(t_2 - t_1)}{V \times \ln(N_2/N_1)} \sum_{i=20}^{34} \frac{z_{i+1} - z_i}{t_{i+1} - t_i}\, dz \tag{6}$$

As shown in Fig. 3, the relationship between the depth of interaction and the photopeak centroid is approximately linear in the center region of the detector. Therefore, depths of interaction ranging from 7.5 mm to 13.125 mm were used to determine

values for τ_e and $\mu_e\tau_e$ using York's solution to a linear least squares fit with known error in both parameters [8]. A weighting potential correction was performed based on the weighting potential values shown in Fig. 4. The induced charge on an anode pixel is proportional to the difference in weighting potential between the gamma-ray interaction location and the anode surface; therefore, without a correction, pulse heights for interactions near the anode will be underestimated compared against interactions near the cathode.

This provides μ_e, τ_e and $\mu_e\tau_e$ for each of the 121 pixels in the detector. It should be noted that these calculated values are averaged over all interaction depths within each pixel. These values can then be averaged to determine the value for all three parameters for an entire detector. The uncertainty in $\mu_e\tau_e$ is also determined for each pixel based on the measured depth uncertainty within the device and the statistical uncertainty of determining the photopeak centroid at each depth [9]. The depth uncertainty is less than 1 mm, but a 1 mm depth uncertainty was used as a conservative estimate. Propagation of error was used to determine the overall uncertainty in $\mu_e\tau_e$.

3. Results

Measured values for μ_e, τ_e and $\mu_e\tau_e$ for two $2\times2\times1.5\ cm^3$ CdZnTe detectors made by Redlen Technologies, Inc. were determined using the methodology explained above. These have been compared against the method described in Ref. [2] in Table 1. The uncertainty in $\mu_e\tau_e$ for Detector #1 and Detector #2 were measured to be 0.03×10^{-2} cm^2/V and 0.01×10^{-2} cm^2/V, respectively. The comparability between the values from each method verifies the accuracy of this new method. This new method has the advantage of determining both μ_e and τ_e. Measured values of $\mu_e\tau_e$ range from 0.5×10^{-2} to 3.2×10^{-2} cm^2/V. Measured values of τ_e range from 10 to 53 μs. Measured values of μ_e range from 0.014×10^{-2} to 0.085×10^{-2} cm^2/V μs. The variation in μ_e is slightly larger than expected and can be attributed to the non-linearity in the electric field; however, it does not appear that these variations cause a larger than expected variation in $\mu_e\tau_e$.

Since this method uses data taken during the standard calibration, it is possible to analyze trends relating the relative electron trapping within a detector to its performance. In Fig. 5, it can be seen that there is a correlation between the electron trapping and the raw energy resolution of a device. This is expected as the raw photopeak will fall in a different amplitude bin for a full energy event near the cathode compared to an event in the middle of the active volume, which is also different from an event near the anode. These differences cause a spread in the overall spectrum. However, the 3D energy reconstruction can correct for the degradation since there is no obvious correlation between the amount of electron trapping and the corrected energy resolution in Fig. 6. This is achievable since the correction is performed for each voxel in the detector, which corrects the electron trapping as a function of depth. This means that the overall spectroscopic performance of a semiconductor detector is independent of the amount of electron trapping present in the detector. A limitation put on this finding is that detectors with severe trapping problems show a correlated poor energy resolution. It was observed that detectors with worse than 6.5% raw FWHM at 662 keV for single pixel events had a corrected energy resolution that was limited by the trapping. However, this is a small fraction of the crystals that have been delivered by Redlen Technologies, Inc [10].

The weak correlation between $\mu_e\tau_e$ and the energy resolution after the 3D position reconstruction can be further exemplified by studying the pixel-by-pixel values of $\mu_e\tau_e$ and energy resolution, as seen in Figs. 7 and 8. It may appear that some regions of the detector show correlation between the two parameters, however, other pixels showing good energy resolution correspond to pixels that have lower values of $\mu_e\tau_e$. The overall trend is that poor energy

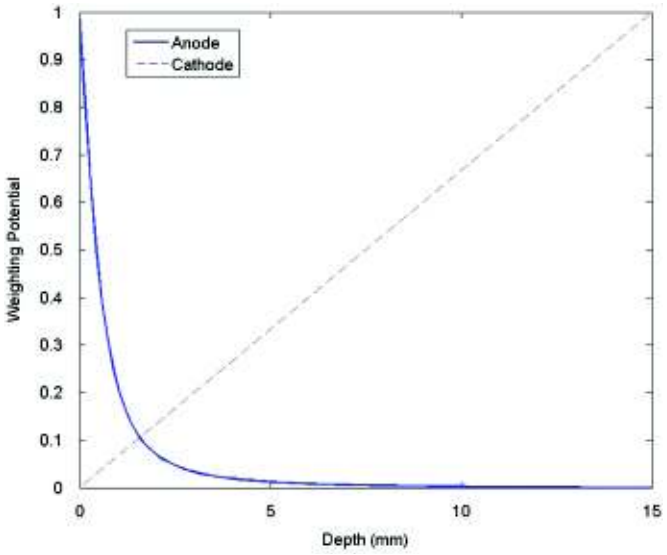

Fig. 4. Weighting potential values for an anode pixel and the planar cathode. The linearity of the cathode weighting potential allows for the use of the cathode-to-anode signal ratio to determine the depth of interaction.

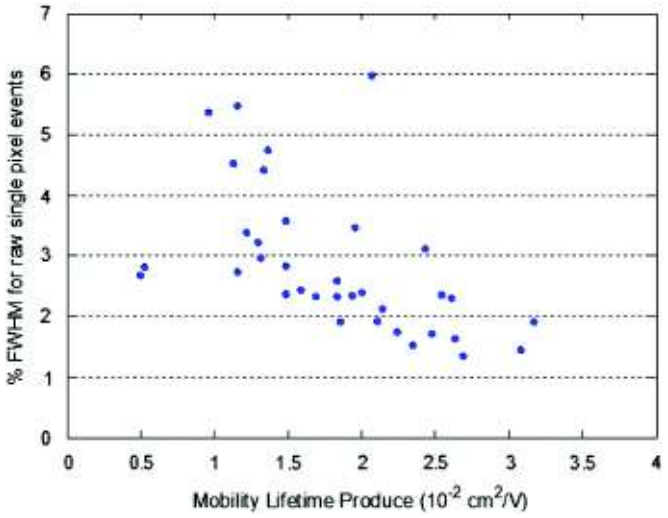

Fig. 5. The $\mu_e\tau_e$ versus raw FHWM of full-energy peak for single pixel events. A linear fit has a correlation coefficient of 0.29.

Table 1
Comparison of values for $\mu_e\tau_e$.

	$\mu_e\tau_e$ ($\times10^{-2}$ cm^2/V)	μ_e ($\times10^{-2}$ $cm^2/V\mu s$)	τ_e (μs)	$\mu_e\tau_e$[a] ($\times10^{-2}$ cm^2/V)
Detector #1	1.27 ± 0.17	0.045 ± 0.005	29.0 ± 0.8	1.41 ± 0.84
Detector #2	1.01 ± 0.09	0.055 ± 0.005	18.5 ± 0.2	1.06 ± 0.30

[a] Using method described in Ref. [2].

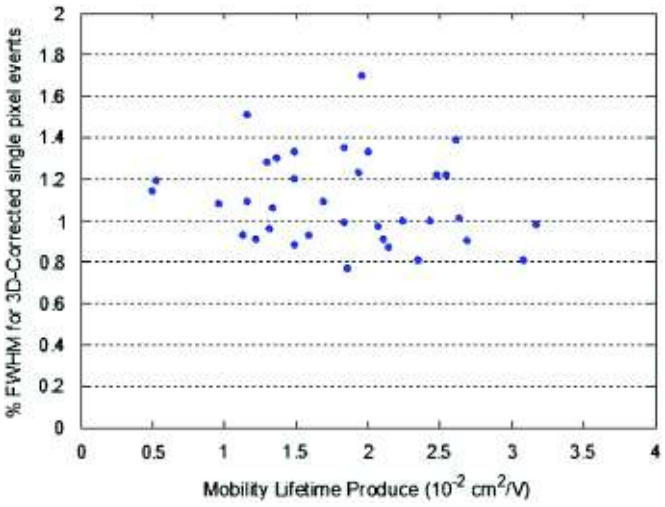

Fig. 6. The $\mu_e\tau_e$ versus corrected FHWM of full-energy peak for single pixel events. A linear fit has a correlation coefficient of 0.04.

5.01	4.01	3.31	3.56	3.83	3.52	3.54	2.99	3.17	3.72	5.23
4.50	3.23	3.19	3.19	2.99	2.65	2.99	2.88	2.96	3.68	2.28
3.49	3.00	2.92	2.61	2.50	2.42	2.39	2.64	2.84	3.26	3.94
3.38	2.85	2.73	2.62	2.55	2.65	2.46	2.78	3.16	2.94	3.65
3.10	2.77	2.40	2.62	2.76	2.61	2.88	2.65	2.54	2.61	3.13
2.85	2.52	2.63	2.58	2.71	2.50	2.50	2.58	2.30	2.40	3.01
2.81	2.54	2.53	2.46	2.61	2.61	2.54	2.50	2.34	2.33	2.78
3.00	2.64	2.54	2.46	2.49	2.75	2.62	2.56	2.47	2.38	2.61
2.71	2.43	2.32	2.29	2.43	2.66	2.42	2.58	2.55	2.57	2.64
2.32	2.13	2.26	2.13	2.41	2.49	2.67	2.56	2.51	2.66	3.02
2.22	2.25	2.36	2.58	2.65	2.90	2.73	2.87	2.88	3.29	3.16

Fig. 7. The $\mu_e\tau_e$ for each of the 121 pixels in an example CdZnTe detector. $\mu_e\tau_e$ has units of 10^{-2} cm^2/V.

0.98	1.06	1.07	1.34	1.01	1.03	1.23	0.88	0.99	1.25	1.30
1.14	1.07	0.94	1.05	1.03	0.89	0.91	0.88	1.00	1.03	0.00
1.01	0.95	1.10	0.91	0.90	0.91	1.08	0.88	0.86	0.97	1.04
0.95	0.90	1.15	0.81	0.89	0.93	0.88	0.88	0.84	0.81	0.94
0.99	0.85	0.83	0.84	0.83	1.02	1.31	0.81	0.79	0.82	0.85
0.90	0.86	0.80	0.80	0.83	0.91	1.00	0.88	1.10	0.81	0.84
0.96	0.88	0.86	0.82	0.79	0.81	0.80	0.85	0.93	0.81	0.87
0.84	0.78	0.78	0.84	0.99	0.76	0.79	0.76	0.81	0.83	0.79
0.84	0.93	0.92	0.92	0.88	0.85	1.11	0.82	0.91	0.90	1.26
0.90	0.86	0.84	0.81	0.81	0.82	0.81	0.83	0.80	0.89	0.85
0.87	0.88	0.82	0.89	0.81	0.77	0.76	0.82	0.83	0.90	0.90

Fig. 8. The 3D corrected energy resolution for single pixel events (in % FWHM at 662 keV) for each of the 121 pixels in an example CdZnTe detector.

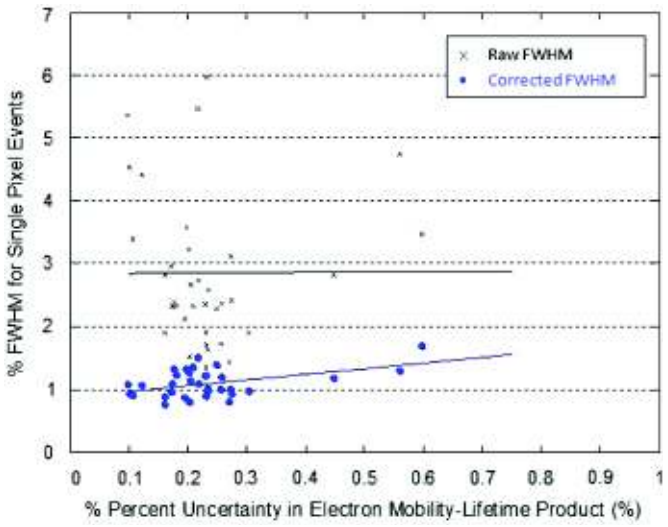

Fig. 9. Percent uncertainty in $\mu_e\tau_e$ versus raw and corrected FHWM for single pixel events. A linear fit for the raw FWHM has a correlation coefficient of 0.00002 while a linear fit for the corrected FWHM has a correlation coefficient of 0.2.

resolution can be found in pixels that show a larger variation in the trapping compared with the surrounding pixels. To better understand this perceived relationship, the measured uncertainty in $\mu_e\tau_e$ is compared against both raw and corrected energy resolution for single pixel events at 662 keV. The results in Fig. 9 show that there is a good correlation between corrected energy resolution and $\mu_e\tau_e$ uncertainty, whereas there is poor correlation between raw energy resolution and $\mu_e\tau_e$. These results are expected. The uncertainty in the measured value of $\mu_e\tau_e$ is determined by several factors. The uncertainty in the depth of interaction and the statistical uncertainty in the photopeak centroid at each depth contribute to the uncertainty for $\mu_e\tau_e$ in each pixel. Larger fluctuations in this uncertainty will correspond to inconsistent trapping, causing an abnormal spread to the amplitude distribution at each depth within the pixel. This increases the uncertainty in the photopeak centroid, which causes an increased uncertainty in the value of $\mu_e\tau_e$ for the pixel. A second factor that can increase the overall uncertainty for in $\mu_e\tau_e$ is the pixel-by-pixel fluctuation in the electron trapping. Larger than expected variations between pixels would cause an increased uncertainty in the averaged value of $\mu_e\tau_e$. These variation would not be expected to impact the raw energy resolution as this is dominated by the first order effect of the overall trapping within the device. The corrected energy resolution fluctuates with these variations since the calibration will either over or under-correct the events that showed the larger trapping variations.

4. Conclusions

A new method has been created to study the electron transport characteristics of single polarity, pixelated semiconductor detectors. This method utilizes the signal deficit from electron

trapping to measure both τ_e and $\mu_e\tau_e$ during the calibration process. The value of μ_e is determined through uniquely mapping the depth of interaction to the drift time. The results are shown to be comparable to the values determined in other studies of material from the same manufacturer [3].

This technique requires single polarity charge sensing, a pixelated anode, a sufficiently long drift time compared to the detector's timing resolution, and a detector thickness that is large compared to the pixel pitch. However, it is not subject to the pitfalls that inhibit the methods based on the Hecht relation or to problems such as the dependence of trapping along the horizontal directions. Actually, this technique will measure the degree to which a detector is subject to non-uniform trapping along the horizontal directions as values of $\mu_e\tau_e$ are found for all 121 pixels. These values are found using standard calibration measurements, allowing for easy comparisons between electron transport properties and overall spectroscopic performance for many detectors. These comparisons have shown that spectroscopic performance is independent of the amount of electron trapping in a device if the raw electron trapping is less than 6.5% from the cathode to the anode surface—this amount of electron trapping corresponds experimentally to a $\mu_e\tau_e$ of approximately 1×10^{-2} cm^2/V and a raw FWHM at 662 keV of approximately 5%. Finally, this technique is not limited to only CdZnTe detectors, but can also be used for other pixelated semiconductor detector such as HgI_2 or TlBr.

Acknowledgments

This work has been jointly supported by DTRA of the Department of Defense and the Department of Energy NA-22 Office.

The authors would like to thank Dr. JaeCheon Kim for providing the weighting potential correction parameters used in the calculation of $\mu_e\tau_e$.

References

[1] T. Schlesinger, R. James, Semiconductors for Room Temperature Nuclear Detector Applications, Series. Semiconductors and Semimetals, Academic Press, 1995 [Online]. Available: 〈http://books.google.com/books?id=v2Zi0Pw54zUC〉.
[2] Z. He, G.F. Knoll, D.K. Wehe, Journal of Applied Physics 84 (10) (1998) 5566.
[3] M. Amman, J. Lee, P. Luke, H. Chen, S. Awadalla, R. Redden, G. Bindley, IEEE Transactions on Nuclear Science NS-56 (3) (2009) 795.
[4] H.Y. Cho, J.H. Lee, Y.K. Kwon, J.Y. Moon, C.S. Lee, Journal of Instrumentation 6 (01) (2011) C01025.
[5] F. Zhang, Z. He, IEEE Transactions on Nuclear Science NS-53 (2006) 3021.
[6] F. Zhang, Events Reconstruction in 3-D Position Sensitive CdZnTe Gamma-ray Spectrometers, Ph.D. dissertation, University of Michigan, May 2005.
[7] Z. He, W. Li, G.F. Knoll, D.K. Wehe, J.E. Berry, C.M. Stahle, Nuclear Instruments and Methods in Physics Research Section A 422 (1999) 173.
[8] B.C. Reed, American Journal of Physics 60 (1) (1992) 59.
[9] J.D. Valentine, A.E. Rana, IEEE Transactions on Nuclear Science NS-43 (5) (1996) 2501.
[10] Y. Boucher, F. Zhang, W. Kaye, Y. Zhu, C. Herman, Z. He, Criteria selection for $20\times20\times15$ mm^3 pixelate CdZnTe semiconductor detectors, in: Nuclear Science Symposium Conference Record (NSS/MIC/RTSD), 2010 IEEE, November 2010.